STATISTICAL MODELS FOR CONSTANT FALSE ALARM RATE SHIP DETECTION WITH THE SUBAPERTURE CROSS-CORRELATION MAGNITUDE

Stian Normann Anfinsen and Camilla Brekke

University of Tromsø
Department of Physics and Technology
N-9037 Tromsø, Norway

ABSTRACT

This paper presents statistical models for the subaperture cross-correlation magnitude (SCM), a test statistic for ship detection which can be produced from single-look complex (SLC) synthetic aperture radar (SAR) data. The SCM is extracted from the complex cross-correlation between two subaperture images and provides enhanced contrast between coherent structures, such as marine vessels, and sea clutter. A modified SCM algorithm has been proposed, which introduces an antialiasing filter in order to allow overlapping sublook spectra. The consequences for the statistical modelling are discussed. We perform an empirical study which validates the use of the K distribution and the Fisher distribution as probability density functions for sea clutter in SCM images. This lays the groundwork for constant false alarm rate (CFAR) detection with SCM images. The fit of the models are assessed with real data.

***Index Terms*—** Synthetic aperture radar, detection algorithms, marine vehicles, subaperture processing

1. INTRODUCTION

The SCM is a high resolution SAR image product which greatly enhances the contrast between ship targets and sea clutter. It is produced by computing a complex cross-correlation or unnormalised coherence between two sublooks that are extracted from an SLC SAR measurement by subaperture processing. The magnitude of this cross-correlation is used as the test statistic, for instance in a CFAR detection algorithm. The increased contrast relies on the short decorrelation time of sea clutter due to wave ripple on the scale of the radar wavelength, as compared to ships, whose man-made structures remain highly coherent within the exposure time of the radar resolution cell. The improved detection performance can also be seen as a result of the SCM incorporating both amplitude and phase information.

The subaperture correlation principle was introduced and the first results presented by Arnaud [1], who referred to it as an interferometric method. The algorithm was then elaborated for both the single polarisation and the polarimetric case by Souyris et al. [2], who referred to the test statistic as the two-look internal Hermitian product (2L-IHP). The early work on the SCM technique covers the frequency domain processing involved in the subaperture extraction, the mathematical analysis of the proposed observables, as well as documentation of the improved target-to-clutter ratio obtained. In this study we extend this with a statistical analysis of the SCM data, which forms the basis for constant false alarm rate (CFAR) detection in SCM images. The subject of the statistical modelling is the output of a modified SCM algorithm recently proposed by the authors [3].

To the best of our knowledge, the distribution of the SCM has not been addressed previously. In the current study, we have first approached the modelling by attempting to utilise distributions for single-look and multilook complex correlations between polarimetric channels, as derived by Tough et al. [4]. This was done in the belief that these should apply equally well to complex correlations between subaperture channels in the same polarisation. It has become clear that the SCM processing is too involved for this simple analogy to apply. It introduces data transformations that cannot easily be followed through in the derivation of the density model. As a resort, we have turned to empirically motivated distributions. The K distribution and the Fisher distribution are found to be flexible enough to capture various circumstances, such as the presence of different levels of radar texture and variations of the processing parameters like the overlap of the subaperture spectra.

Section 2 describes the SCM product, both the classical definition from [2] and the modified version proposed in [3]. The suggested density models are introduced in Section 3 together with their parameter estimation procedures. The goodness-of-fit of the models are evaluated in Section 4, before conclusions are given in Section 5.

2. DATA PROCESSING

2.1. Subaperture Cross-correlation Magnitude Product

Let S be the complex scattering coefficient measured by a single polarisation SAR instrument. Further assume that S_1

and S_2 are the scattering coefficients representing two subapertures that can be extracted from SLC data by splitting the azimuth spectrum into subbands and focusing them separately [1, 2]. The splitting can in principle also be done with the range spectrum, but Doppler domain splitting has proven empirically to produce the best results [5].

The complex cross-correlation between the subapertures are computed as the Hermitian inner product: $\rho = S_1 \cdot S_2^*$, where the superscripted $*$ denotes complex conjugation. The SCM product is formed in the same way as an interferometric coherence, by averaging over a local neighbourhood. Let the single polarisation SCM be defined as

$$r = |\rho_n| = |\langle S_1 \cdot S_2^* \rangle_n| \tag{1}$$

where $\langle \cdot \rangle_n$ means spatial averaging over n pixels and ρ_n is the averaged complex cross-correlation.

2.2. Modified Algorithm

The bandwidth splitting has conventionally been done by extracting two subbands that together share the available bandwidth, possibly separated by a small guard interval to avoid correlation and aliasing [2, 5]. Nonetheless, already in his seminal paper, Arnaud [1] launched the idea of varying the subaperture bandwidth and the separation of the subbands depending on the sea state to optimise the contrast. As a response to this, a range of different subband extraction strategies have been evaluated in [3]. To accomodate overlapping subbands, a modified SCM processing algorithm is also proposed, whose main feature is to include an antialiasing filter which is required in the case of spectral overlap between the subapertures. The procedure involves resampling and lowpass filtering of the image data in the frequency domain, which naturally modifies the statistical characteristics of the resulting image product.

The results obtained in [3] suggest that the highest target-to-clutter ratios are obtained with overlapping subbands. Another argument for allowing subband overlap is that the spatial resolution of the SCM product improves as the subaperture bandwidth increases. Hence, the statistical modelling is targeted at the output of the modified SCM algorithm.

3. STATISTICAL MODELS

3.1. A Distribution Based on the Signal Model

With a signal model as described by (1), it would be natural to look to the literature for known distributions of similar complex correlations. Indeed, Tough et al. have already derived various distributions related to the complex cross-correlation between polarimetric channels, covering both the magnitude and phase, and the single-look as well as the multilook case [4]. These derivations make the assumption that the scattering coefficients follow a joint circular complex and zero mean Gaussian distribution.

The cross-correlation between subapertures should in principle not be very different from cross-correlation between polarimetric channels. Therefore, the distribution of the multilook Hermitian product amplitude [4, Eq. (67)] was hypothesised as a model for r, with pdf

$$\begin{aligned} p_r(r; k, \psi) = {} & \frac{4n(nr)^n}{\psi^{n+1}(1-k^2)\Gamma(n)} \\ & \times I_0\left(\frac{2knr}{\psi(1-k^2)}\right) K_{n-1}\left(\frac{2nr}{\psi(1-k^2)}\right) . \end{aligned} \tag{2}$$

Here $I_m(r)$ and $K_m(r)$ are the modified Bessel functions of the first and second kind, respectively, with order parameter m. The pdf is parametrised by the geometric mean subaperture intensity, $\psi = \left(\mathrm{E}\{|S_1|^2\}\,\mathrm{E}\{|S_2|^2\}\right)^{1/2}$, and the subaperture coherence, $k = \mathrm{E}\{\rho\}/\psi$.

When this hypothesis was put forward, we expected that the increasing degree of correlation introduced by overlapping subbands could be modelled in much the same way as channel correlations. However, tests with real data have shown that the density model in (2) does not provide an adequate model for the SCM product. There are several parts to the explanation. The frequency domain processing of the modified SCM algorithm introduces data transformations that are not accounted for by the model. Moreover, the spatial averaging in (1) produces SCM pixels with considerable correlation. In addition, the model should cope with the pronounced radar texture experienced in rough sea states, but (2) is derived for Gaussian sublook scattering coefficients. A product model extension of (2) to incorporate texture is possible, but it does not yield closed form expressions for the probability density function (pdf), which must therefore be evaluated by numerical integration [4].

3.2. Empirical Distributions

The proposed solution is to use density models that are not derived from the signal model, but heuristically chosen based on their flexibility and on experimental validation. We took the gamma distribution as a starting point, and found it to produce acceptable fit to the SCM data when the sea clutter is homogeneous and there is little spectral overlap between the sublooks. We then proceeded with the K distribution and the Fisher distribution, that are extensions of the gamma distribution, to obtain the flexibility required to handle different sea states and processing parameters.

Remark that empirical distributions with high versatility will allow us to model SCM data produced in different ways. For instance, the test statistic used in [2] was formed as the incoherent sum of two SCMs obtained by splitting the azimuth spectrum and the range spectrum, respectively. The modelling of this statistic has not been attempted in our study.

We now turn to the candidate density models for r.

3.2.1. Gamma Distribution

Let $\Gamma[\mu, L]$ denote a gamma distribution with location parameter $\mu > 0$ and shape parameter $L > 0$, whose pdf is [6]

$$p_r(r; \mu, L) = \frac{1}{\Gamma(L)} \frac{L}{\mu} \left(\frac{Lr}{\mu} \right)^{L-1} \exp\left\{ -\frac{Lr}{\mu} \right\} \quad (3)$$

where $\Gamma(\cdot)$ is Euler's gamma function.

3.2.2. Inverse Gamma Distribution

The inverse gamma distribution is denoted $\Gamma^{-1}[\mu, L]$, with the same parameters as in $\Gamma[\mu, L]$. The pdf is [6]

$$p_r(r; \mu, L) = \frac{1}{\Gamma(L)} \frac{1}{L\mu} \left(\frac{L\mu}{r} \right)^{L+1} \exp\left\{ -\frac{L\mu}{r} \right\} . \quad (4)$$

This distribution can be used together with $\Gamma[\mu, L]$ as a building block to form composite distributions with higher flexibility.

3.2.3. K Distribution

The product of two gamma distributed variables follows the K distribution, denoted $K[\mu, L, M]$, with M as an additional shape parameter. The pdf can be expressed as the Mellin convolution of two gamma distributions: $K[\mu, L, M] = \Gamma[\mu, L] \hat{\star} \Gamma[1, M]$, which becomes [6]

$$p_r(r) = \frac{2}{\Gamma(L)\Gamma(M)} \frac{LM}{\mu} \left(\frac{LMr}{\mu} \right)^{\frac{L+M-2}{2}} \times K_{M-L}\left(2\sqrt{\frac{LMr}{\mu}} \right) . \quad (5)$$

3.2.4. Fisher Distribution

The quotient of two gamma distributed variables follows the Fisher distribution, denoted $F[\mu, L, M]$. The pdf can be expressed as $F[\mu, L, M] = \Gamma[\mu, L] \hat{\star} \Gamma^{-1}[1, M]$, which evaluates to [6]

$$p_r(r) = \frac{L}{M\mu} \frac{\Gamma(L+M)}{\Gamma(L)\Gamma(M)} \frac{\left(\frac{Lr}{M\mu} \right)^{L-1}}{\left(1 + \frac{Lr}{M\mu} \right)^{L+M}} . \quad (6)$$

3.3. Parameter Estimation

We use method-of-moments type estimators for all parameters. The location parameters of the models are estimated from the first-order moment. The shape parameters are estimated from the logarithmic moments known as log-cumulants. The relevant moment expressions can be found in [6]. Inversion of the log-cumulant equations must be done with a numerical optimisation algorithm.

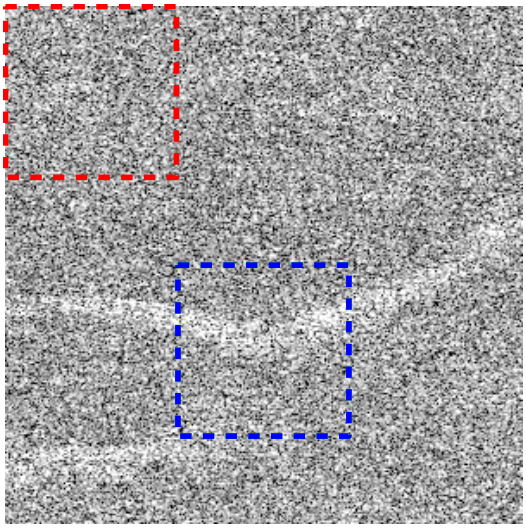

Fig. 1. HV channel intensity from Radarsat-2 image of Boknafjorden, Norway, with test areas A and B indicated in red and blue ().

4. RESULTS

Fig. 1 shows parts of a full-polarimetric Radarsat-2 scene acquired on 27 October 2011 over Boknafjorden, Norway, in wind conditions that were forecasted to a speed of 10-15 m/s. The image contains no targets, but has some oceanographic features that cause nonstationary backscatter statistics, which is clearly seen in the displayed HV channel intensity.

Sea clutter is selected from two test areas. Area A is shown as the red box and area B as the blue box in Fig. 1. These are chosen such that area A is relatively homogeneous, whereas area B is heterogeneous with statistics that are clearly varying spatially. Adequate models would be expected to cover such variability.

SCM data have been produced with subaperture bandwidths that take up a fraction β of the available bandwidth, and β has been varied from 0.3 to 1.0, which is found to be the viable range [3]. The models $\Gamma[\mu, L]$, $K[\mu, L, M]$ and $F[\mu, L, M]$ have then been fitted to the data. Fig. 2 shows the results for the HH channel SCM product in test area A with $\beta = 0.8$. Fig. 3 shows the results for the HV channel SCM in test area B with $\beta = 0.6$. The pdfs are shown on both linear and semilogarithmic scale to emphasise the model behaviour in the head and tail of the distributions, respectively. The pdfs of the gamma distribution (green), K distribution (red) and Fisher distribution (blue) are plotted on top of the SCM data histogram (yellow). Note that the data have been rescaled to unit mean before fitting for visualisation purposes.

The gamma distribution overall provides a reasonably good fit for the head of the data distribution, but cannot capture the heavy tails. The K distribution produces a very good

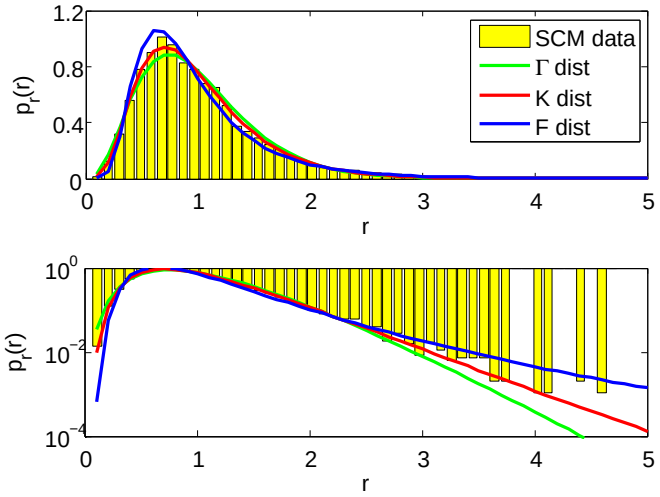

Fig. 2. Modelling of HH channel SCM in test area A with sublook bandwidth fraction $\beta = 0.8$.

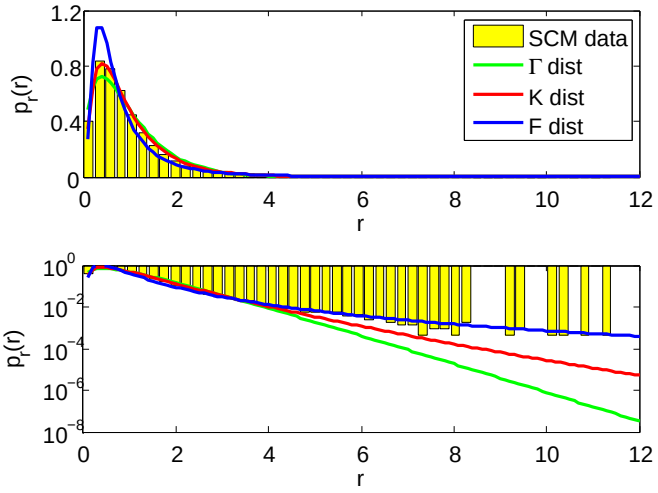

Fig. 3. Modelling of HV channel SCM in test area B with sublook bandwidth fraction $\beta = 0.6$.

fit both in the head and the tail as long as the sea clutter is not too heterogeneous. In the latter case it fails to model the heavy tail, as seen in Fig. 3. The Fisher distribution generally does not fit the head very well, and also produces an excessively heavy tail when the sea clutter is homogeneous, as seen in Fig. 2. It has its strength in the tail modelling for heterogeneous data, with Fig. 3 as an example.

5. CONCLUSIONS

The important aspect for CFAR ship detection is accurate modelling of the tail of the SCM distribution. Our experiments show that this can be achieved with a K distribution model in homogenous to moderately heterogeneous sea clutter. When the sea clutter is very heterogenous, which could be caused by nonstationary backscatter statistics, we may rely on the Fisher distribution. This suggests that a dictionary approach should be adopted, which selects between the two models based on a goodness-of-fit test. Alternatively, we may use the four-parameter U distribution, which contains the K distribution and the Fisher distribution as special cases [6]. However, the flexibility comes at the cost of increased estimation uncertainty. Other models, such as the generalised gamma distribution [7], should therefore also be investigated. In our further work we will incorporate formal goodness-of-fit tests of the candidate models, and use this to device an operational algorithm which automatically selects the appropriate model based on the statistical characteristics of the SCM data.

6. REFERENCES

[1] A. Arnaud, "Ship detection by SAR interferometry," in *Proc. Int. Geosci. Remote Sens. Symp., IGARSS 1999*, vol. 5, Hamburg, Germany, 28 June-2 July 1999, pp. 2616–2618.

[2] J.-C. Souyris, C. Henry, and F. Adragna, "On the use of complex SAR image spectral analysis for target detection: Assessment of polarimetry," *IEEE Trans. Geosci. Remote Sens.*, vol. 41, no. 12, pp. 2725–2734, Dec. 2003.

[3] C. Brekke, S. N. Anfinsen, and Y. Larsen, "A study of sublook extraction strategies in ship detection with the sublook correlation magnitude," *IEEE Geosci. Remote Sens. Lett.*, 5 pp., submitted.

[4] R. J. Tough, D. Blacknell, and S. Quegan, "A statistical description of polarimetric and interferometric synthetic aperture radar data," *Proc. R. Soc. London A*, vol. 449, no. 1937, pp. 567–590, Jun. 1995.

[5] H. Johnsen and Y. Larsen, "A novel method for spaceborne SAR vessel detection using complex radar backscatter," Norut IT, Tromsø, Norway, Tech. Rep. 12/2005, Dec. 2006.

[6] J.-M. Nicolas, "Application de la transformée de Mellin: Étude des lois statistiques de l'imagerie cohérente," Ecole Nationale Supérieure des Télécommunications, Paris, France, Tech. Rep. 2006D010, 2006, in French.

[7] H.-C. Li, W. Hong, Y.-R. Wu, and P.-Z. Fan, "On the empirical-statistical modeling of SAR images with generalized gamma distribution," *IEEE J. Sel. Topics Signal Process.*, vol. 5, no. 3, pp. 386–397, Jun. 2010.